ADVANCED OPTICAL MATERIALS
www.advopticalmat.de

Determining the Width of the Dynamic Emission Zone in Light-Emitting Electrochemical Cells

*Xiaoying Zhang, Joan Ràfols-Ribé, Anton Kirch, Christian Larsen, and Ludvig Edman**

The light-emitting electrochemical cell (LEC) forms a p-n junction doping structure by bipolar electrochemical doping during its initial operation. The light emission originates from the p-n junction region through the formation and radiative decay of excitons. The width of this emission zone (EZ) is important since it strongly affects the emission losses by exciton quenching, the outcoupling efficiency, and the drive voltage. The challenge is that it has proven very difficult to determine the width of the dynamic EZ in LECs. Here, this issue is addressed through the presentation of a method that fits simulated angle-resolved emission spectra to measured spectra, using the EZ width and position as the two free parameters. For improved accuracy, a linear polarizer is employed for the selective detection of s-polarized emission and a half-cylinder outcoupling structure for enhanced spectral output. The method is finally employed on a common conjugated-polymer LEC, and it is derived that its EZ width decreases during the initial operation, that the steady-state EZ width is equal to ≈20% of the active-material thickness at a current density of 10 mA cm^{-2}, and that the steady-state EZ width appears to decrease with increasing current density.

1. Introduction

The light-emitting electrochemical cell (LEC) is attracting increasing interest since it can deliver bright area emission at low voltage from thin and flexible devices,[1–14] and since it can be fabricated by energy- and cost-efficient printing and coating under ambient air.[15–17] An LEC essentially consists of two electrodes that sandwich a single layer of emissive active material, with the latter comprising an electroluminescent organic semiconductor and mobile ions.[18–21] When a voltage is applied between the electrodes, the mobile ions redistribute to form electric double layers (EDLs) at the two electrode interfaces, which facilitates efficient and balanced injection of electrons and holes into the organic semiconductor. The first injected electrons and holes are electrostatically compensated through the redistribution of the remaining mobile ions in the active material; in other words, electrochemical p-type doping forms at the anode and electrochemical n-type doping at the cathode.[22] These two doping regions grow and form a p-n junction, where subsequently injected electrons and holes recombine into excitons; these excitons can decay radiatively through the emission of photons.[23]

The emission zone (EZ) is thus akin to the p-n junction, and its detailed structure has been demonstrated to have a profound impact on the LEC performance. For example, the EZ position determines whether the LEC is operating at constructive or destructive interference,[24–26] the EZ width has a strong influence on the emission losses to exciton-polaron and exciton-exciton quenching,[27,28] while the combined width and position of the EZ determine the impact of the (typically lossy) coupling of the excitons to surface plasmon-polariton modes at the electrode interfaces.[29] In addition, a wider EZ is concomitant with a higher drive voltage, since the p-n junction is the most resistive part of the LEC structure (at steady state).

It is thus clear that it is highly desired and motivated to develop methods for the determination of the EZ structure in LEC devices, but also that this endeavor is rendered complicated by the fact that the doping structure, and thereby the EZ, forms and develops in situ during LEC operation. This is in contrast to the situation in organic light-emitting diodes (OLEDs), where a desired static doping structure is established during device fabrication, and where the EZ structure can be accurately determined by spectrogoniometer measurements, optical simulations, and fitting algorithms.[30,31] In LECs, the average EZ position has been determined with high accuracy by the fitting of simulated

X. Zhang, J. Ràfols-Ribé, A. Kirch, C. Larsen, L. Edman
Department of Physics
The Organic Photonics and Electronics Group
Umeå University
Umeå SE-90187, Sweden
E-mail: ludvig.edman@umu.se
J. Ràfols-Ribé, C. Larsen, L. Edman
LunaLEC AB
Umeå University
Umeå SE-90187, Sweden
L. Edman
Wallenberg Initiative Materials Science for Sustainability
Department of Physics
Umeå University
Umeå SE-90187, Sweden

The ORCID identification number(s) for the author(s) of this article can be found under https://doi.org/10.1002/adom.202501128

DOI: 10.1002/adom.202501128

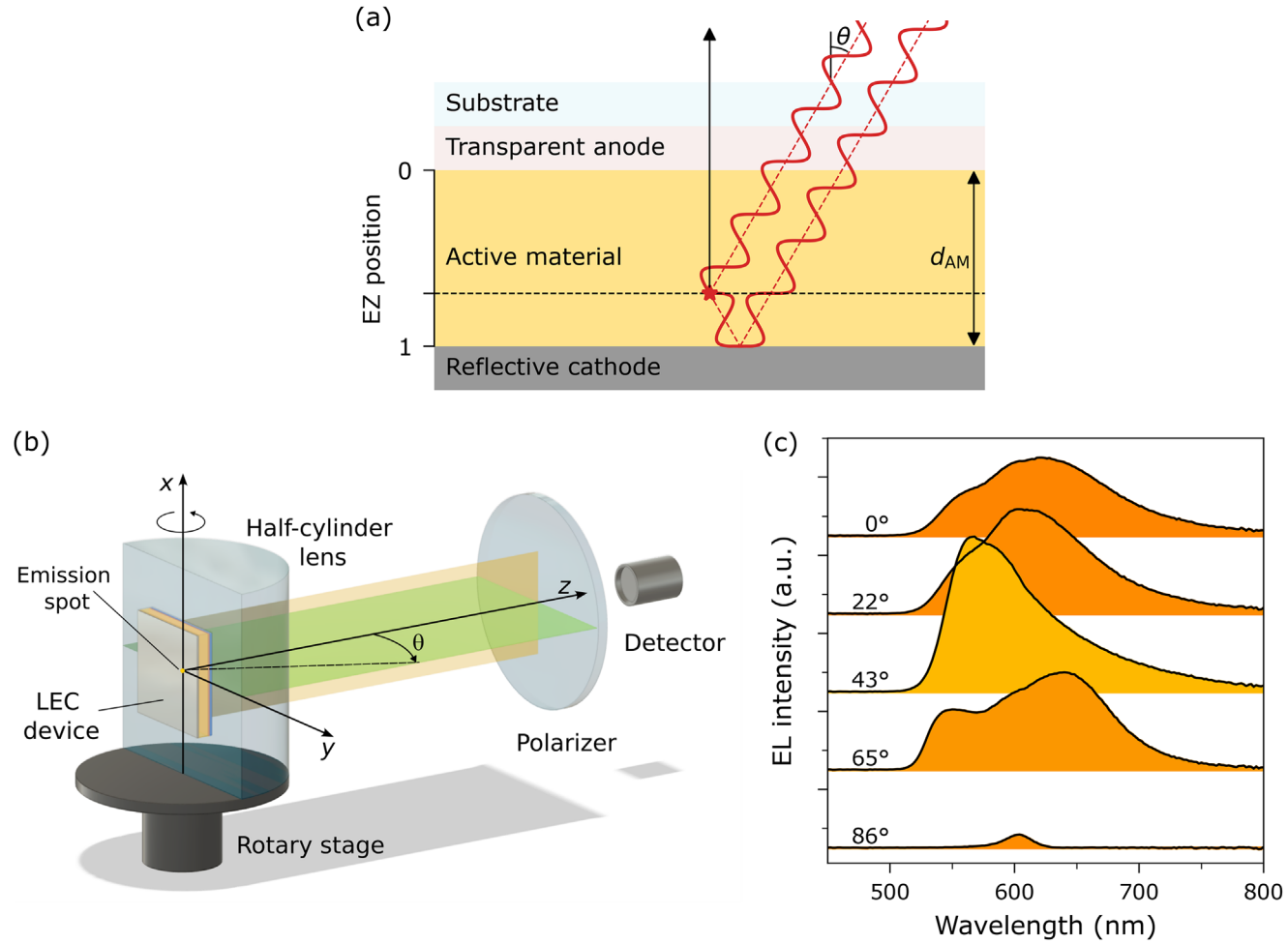

Figure 1. a) Schematic presentation of the LEC device structure and the microcavity effect that is utilized for the determination of the EZ parameters; note that the refraction at the interfaces has been excluded for clarity. b) Schematic presentation of the spectrogoniometer setup, with a half-cylinder outcoupling structure attached on the transparent substrate of the LEC device, and a linear polarizer included before the detector. The emission angle with respect to the device normal that is measured by the detector is θ. c) The measured steady-state EL spectrum of an LEC device as a function of θ during steady-state operation at a current density of 50 mA cm^{-2}.

emission spectra to measured emission spectra.[32] However, the determination of the EZ width suffers from a much poorer accuracy and/or questionable assumptions, although we note that some information has been gleaned from impedance spectroscopy measurements[25,33,34] and drift-diffusion modeling.[35]

Here, we address this issue by presenting a method for the in situ determination of the evolution of the EZ width during LEC operation. We specifically fit simulated angle-resolved emission spectra to corresponding measured spectra, with the EZ position and the EZ width as the two free fitting parameters. The simulated spectra were derived using previously established electrochemical-doping-dependent material properties, while the measured spectra were recorded with a half-cylinder sphere positioned on the transparent part of the device for improved outcoupling and a linear polarizer positioned before the detector for the selective detection of the s-polarized emission. By systematically executing this method on a common conjugated-polymer LEC, we could establish that the EZ width is decreasing during the initial turn-on process, that the steady-state EZ width is ≈20% for a device with an active-material thickness of 300 nm when driven by a constant current density of 10 mA cm^{-2}, and that the steady-state EZ width is decreasing with increasing current density.

2. Results and Discussion

Figure 1a presents a schematic of the employed LEC structure, comprising a transparent indium-tin-oxide (ITO) anode on a transparent glass substrate and a reflective Al cathode sandwiching a single layer of active material. The active material consists of an optimized blend of the electroluminescent conjugated polymer Super Yellow (SY), the salt KCF_3SO_3, and the ion transporter hydroxyl-capped trimethylolpropane ethoxylate (TMPE-OH).[23,33,35,36] The thickness of the active material (d_{AM}) is selected to be 300 nm, since this has been demonstrated to result in that this particular device structure, as desired for the herein utilized method, can be operated close to minimum optical outcoupling.[36,37] More details on the device fabrication can be found in the Experimental Section.

The EZ position in the active material (or interelectrode gap) is indicated by the horizontal dotted black line in Figure 1a, and it is normalized with respect to d_{AM}, with 0 indicating the anodic interface and 1 the cathodic interface. Two light waves (wavy red lines in Figure 1a) are presented that both originate in the same spot in the EZ and that both exit the device structure with the same emission angle θ; but which are distinguished by that the first wave is directed toward the transparent anode/substrate, whereas the second wave first is reflected off the cathode. The interaction of these two light waves visualizes part of the microcavity effect, which can be prominent in thin-film devices.[31,38] More specifically, in our system, the two light waves will interfere constructively when the optical path difference is an integer multiple of the wavelength (i.e., the two waves are in phase). In contrast, they will interfere destructively when the optical path difference is a half-integer multiple of the wavelength (i.e., the two waves are out of phase). The optical path difference is determined by the distance between the EZ and the reflective (cathodic) interface,[39,40] the refractive index of the active material,[41] the phase shift of the light wave during reflection at the reflective interface,[42] and the emission angle θ.[43,44]

Figure 1b is a schematic of the custom-built spectrogoniometer setup that was employed for the measurement of the angle-resolved electroluminescence (EL) spectrum and intensity.[36] The LEC device under study is placed on a goniometer stage, and its rotation around the x-axis (in the green y-z plane) defines the emission angle θ in air, with 0° corresponding to forward emission. A half-cylinder glass outcoupling structure, with its symmetry axis aligned with the rotation axis of the stage, is attached to the glass substrate of the device with an index-matching oil to suppress losses to substrate modes.[45]

A linear polarizer is placed in front of the detector, and it is oriented to only allow s-polarized light waves (with their electric-field component in the yellow x-z plane) to reach the detector. This procedure simplifies the analysis of data and improves the accuracy of the method, since the s-polarized light wave only includes a contribution from the horizontally oriented emitters (emissive dipoles or excitons) in the active material, whereas the p-polarized light wave includes a contribution from both horizontally and vertically oriented emitters.[36] Thus, the selective detection of the s-polarized light waves eliminates the requirement of identifying the relative proportions of the horizontally and vertically oriented emitters in the active material.

Figure 1c presents an example of the measured s-polarized EL spectrum and intensity from the LEC device (d_{AM} = 300 nm) as a function of the emission angle θ during steady-state operation at a current density of 50 mA cm^{-2}. The observed strong dependency of the EL spectral shape and intensity on θ is a manifestation of that the LEC device, as desired, is shifting between destructive and constructive interference by a mere change of θ.[40,46]

The angle-resolved EL spectrum and intensity of the LEC device were also simulated by the commercial software Setfos, using the EZ position and the EZ width as the two free parameters. **Figure** 2a presents the simulated LEC structure, which, in agreement with the measured LEC, comprises a 300 nm thick layer of active material sandwiched between a 100 nm thick Al cathode and a 145 nm thick ITO anode; the latter is positioned on top of a transparent and infinitely thick (and incoherent) glass layer to mimic the combined effects of the glass substrate and the half-cylinder glass outcoupling structure in the measurements.[36]

Figure 2b displays the simulated steady-state doping concentrations and exciton generation profile in the active material as a function of the normalized interelectrode position. The exciton generation profile is simulated as a Gaussian function (which was shown to be a good approximation in ref. [28]):

$$f(x) = \frac{1}{\sigma\sqrt{2\pi}} e^{-\frac{1}{2}\left(\frac{x-x_0}{\sigma}\right)^2} \quad (1)$$

where x is the normalized interelectrode position, x_0 the Gaussian center position, and σ its standard deviation. x_0 is thus equal to the "EZ position" at which peak exciton generation takes place, whereas the "EZ width" is herein defined to be equal to 6σ. The latter results in that <0.5% of the excitons are generated outside of the EZ in the simulation, and this minor fraction of excitons is removed from further analysis because of a fundamental requirement of the simulation software. The exciton emission spectrum is set equal to the measured photoluminescence spectrum of a 17-nm-thin Super Yellow film.[23]

The doping regions are divided into a ten-sublayer p-type doping region and a ten-sublayer n-type doping region, which sandwich the EZ. The overall doping gradients are constant, with the highest doping concentration at the corresponding injecting electrode and zero doping concentration at the EZ interface. Each of the doping sublayers exhibits constant doping concentration, with the doping- and wavelength-dependent complex refractive index of each such sublayer gleaned from previous measurements.[47,48] The total number of p-type dopants in the p-doping region is set equal to the total number of n-type dopants in the n-type doping region because of charge conservation, and the average doping concentration in the active material is set equal to the initial ion concentration in the experimental devices (i.e., 9.6×10^{19} cm^3).

Figure 2c presents the simulated s-polarized EL spectrum and intensity as a function of the emission angle θ for an LEC device during steady-state operation at a current density of 50 mA cm^{-2}, with the simulated EZ position being 0.59 and the simulated EZ width being 0.16. The EL spectrum and intensity exhibits a strong dependence on θ, and we call attention to the resemblance between the simulated angle-resolved EL data in Figure 2c and the measured angle-resolved EL data in Figure 1c.

The values for the EZ position and width can now be determined by identifying the global minimum of the mean absolute error (MAE) between the measured EL spectral data and the simulated EL spectral data. More specifically, we calculate MAE as a function of the EZ position (=x_0) and the EZ width ($w_0 = 6\sigma$) with the equation:

$$\mathrm{MAE}\ (x_0, w_0) = \frac{1}{N_\theta} \sum_\theta \frac{1}{N_\lambda} \sum_\lambda \left| I^{\mathrm{meas}}_{\theta,\lambda} - I^{\mathrm{sim}}_{\theta,\lambda}\ (x_0, w_0) \right| \quad (2)$$

where $I^{\mathrm{meas}}_{\theta,\lambda}$ is the measured EL spectral intensity as a function of emission angle θ and $I^{\mathrm{sim}}_{\theta,\lambda}(x_0, w_0)$ is the simulated EL spectral intensity as a function of θ. Both the measured and simulated EL intensity are normalized to the maximum EL intensity at 0°. N_θ and N_λ are the number of measured and simulated emission angles (= 17) and emission wavelengths (=176), respectively.

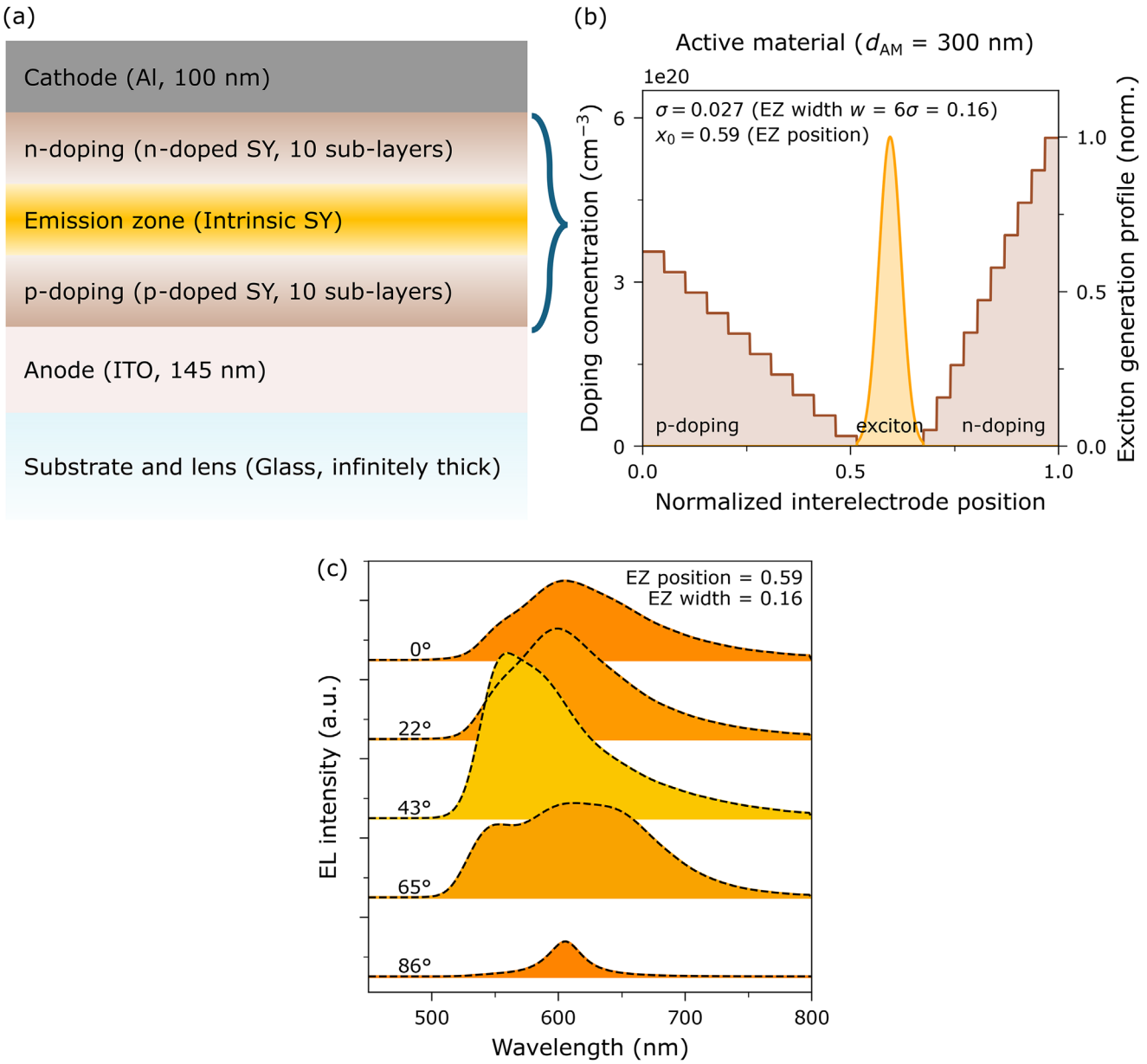

Figure 2. a) The simulated steady-state LEC structure, comprising an active material divided into a p-type doping region, an intrinsic emission zone (EZ), and an n-type doping region. b) The simulated 10-sublayer p-type doping region, the 10-sublayer n-type doping region, and the Gaussian-shaped exciton generation profile in the EZ as a function of the normalized interelectrode position. The presented EZ peak is located at 0.59 and the EZ width is 0.16. c) The simulated s-polarized EL spectrum as a function of θ for the LEC device (d_{AM} = 300 nm) during steady-state operation at a current density of 50 mA cm^{-2}.

Figure 3a presents the derived MAE as a function of the simulated values for the EZ position (horizontal x-axis) and the EZ width (vertical y-axis) for an LEC device that is operating at steady state when driven by a current density of 25 mA cm^{-2}. Steady state is defined to be reached at the time of minimum voltage in the measurement. The identified global minimum for MAE (as indicated by the red star in Figure 3a thus reveals that, for this particular device and operational condition, the best-estimated EZ position is at 0.62 and the best-estimated EZ width is 0.18. For the device with an active-material thickness of d_{AM} = 300 nm, this translates into an EZ center position that is 186 nm away from the transparent anode (and 114 nm away from the reflective cathode) and an EZ width of 54 nm.

Figure 3b shows the local minimum of the MAE as a function of the simulated EZ position, while Figure 3c presents the local minimum of the MAE as a function of the simulated EZ width. Figure 3d finally compares the measured angle-resolved EL spectra (solid lines) with the simulated angle-resolved EL spectra using the derived best estimator values for the EZ position of 0.62 and the EZ width of 0.18 (dashed lines). The observed good replication of the angle-resolved measured EL spectra by the simulation provides confirmation of the validity of the procedure.

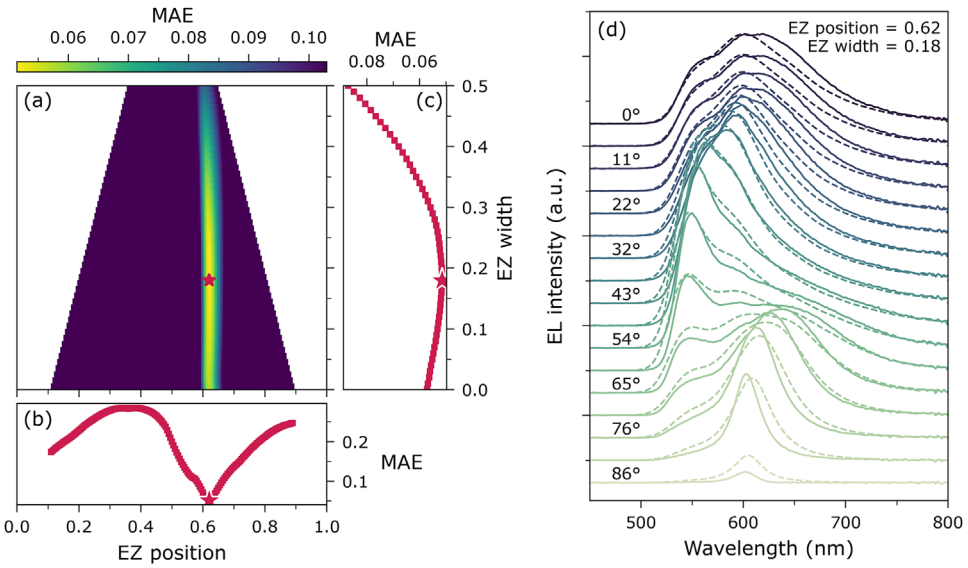

Figure 3. a) 2D color graph of the mean absolute error (MAE) as a function of the simulated values for the EZ position (horizontal x-axis) and the EZ width (vertical y-axis) for an LEC device operating at steady state while driven by a current density of 25 mA cm^{-2}. The red star indicates the global minimum of MAE, which identifies the best-estimated values for the EZ position and the EZ width. b) The local minimum of MAE as a function of the simulated EZ position. c) The local minimum of MAE as a function of the simulated EZ width. d) The measured (solid lines) and best-estimated (dashed lines) EL spectra as a function of θ for the device at steady state when driven with a current density of 25 mA cm^{-2}.

However, a few words of caution are in place, which can serve as inspiration for future research and development. First, the derived value for the global minimum of MAE (EZ position = 0.62, EZ width = 0.18) is 0.05, while it – in the ideal case of a perfect model and a perfect measurement – should be 0. In this context, we mention that the quality of the simulation will be improved when more detailed information on the shape of the doping profiles and the exciton generation zone in the active material becomes available. Second, a comparison between Figure 3b,c reveals that the method identifies the EZ position with a higher accuracy than the EZ width. This can be exemplified by that a small change of the EZ position from 0.62 to 0.64 results in a 20% increase of MAE (see Figure 3b), while the same increase of MAE is concomitant with an increase of the EZ width from 0.18 to 0.35, as gleaned from Figure 3c. Third, we have chosen to, somewhat arbitrarily, define the EZ width as being six times the standard deviation of a Gaussian-shaped exciton generation zone; it is thus important to keep this definition in mind when comparing the herein derived values for the EZ width with values derived with other methods (that plausibly have adopted a different definition). Moreover, direct observations of the EZ in planar surface cells, with much larger interelectrode gaps of 0.1-1 mm, established that the EZ can have a jagged shape with respect to the electrode surface plane,[49–51] which would imply that the herein derived value represents the "average EZ width" while the "local EZ width" is thinner.

We now utilize the presented method for the study of the transient evolution of the EZ in an LEC during its initial operation. **Figure** 4a,b present the temporal evolution of the voltage and the forward luminance, respectively, for three different current densities, as identified in the inset of Figure 4a. The time of steady state (i.e., minimum voltage) is indicated by the solid squares. The derived time evolution of the best-estimated EZ position and the best-estimated EZ width are displayed in Figure 4c,d, respectively; the temporal resolution of slightly more than 1 min is determined by the time required to measure one complete set of angle-resolved EL spectra.

Figure 4c shows that the EZ position is formed closer to the negative cathode (at 0.65–0.70) and thereafter is migrating toward the center of the interelectrode gap during the first hour of operation. The figure also discloses that the entire transient is shifted toward the center of the active material with increasing current density. The corresponding analysis of the EZ-width data in Figure 4d results in two findings: i) the best-estimated EZ width decreases during the initial LEC operation, and ii) the best-estimated steady-state EZ width narrows with increasing current density (and voltage).

In order to investigate whether these observations are consistent, we have characterized nine devices from three different batches. The complete set of characterization data is presented in Figures S1 and S2 (Supporting Information). It is reassuring that the device-to-device variation is rather minor and that the above-identified trends for the best-estimated EZ position and width hold for all devices. We have also investigated the sensitivity of the derived values for the EZ position and the EZ width using the error calculation method presented in ref. [29]. Figure S3 (Supporting Information) confirms that the presented method produces a more exact determination of the EZ position than the EZ width.

Figure 4e,f summarize all derived steady-state values for the best-estimated EZ position and the EZ width, respectively, as a function of the current density. The red horizontal line markers show the mean of all these values for the EZ position and the EZ width, while the black rectangles show the corresponding population standard deviation. It is clear that this summary plot confirms the trends presented above.

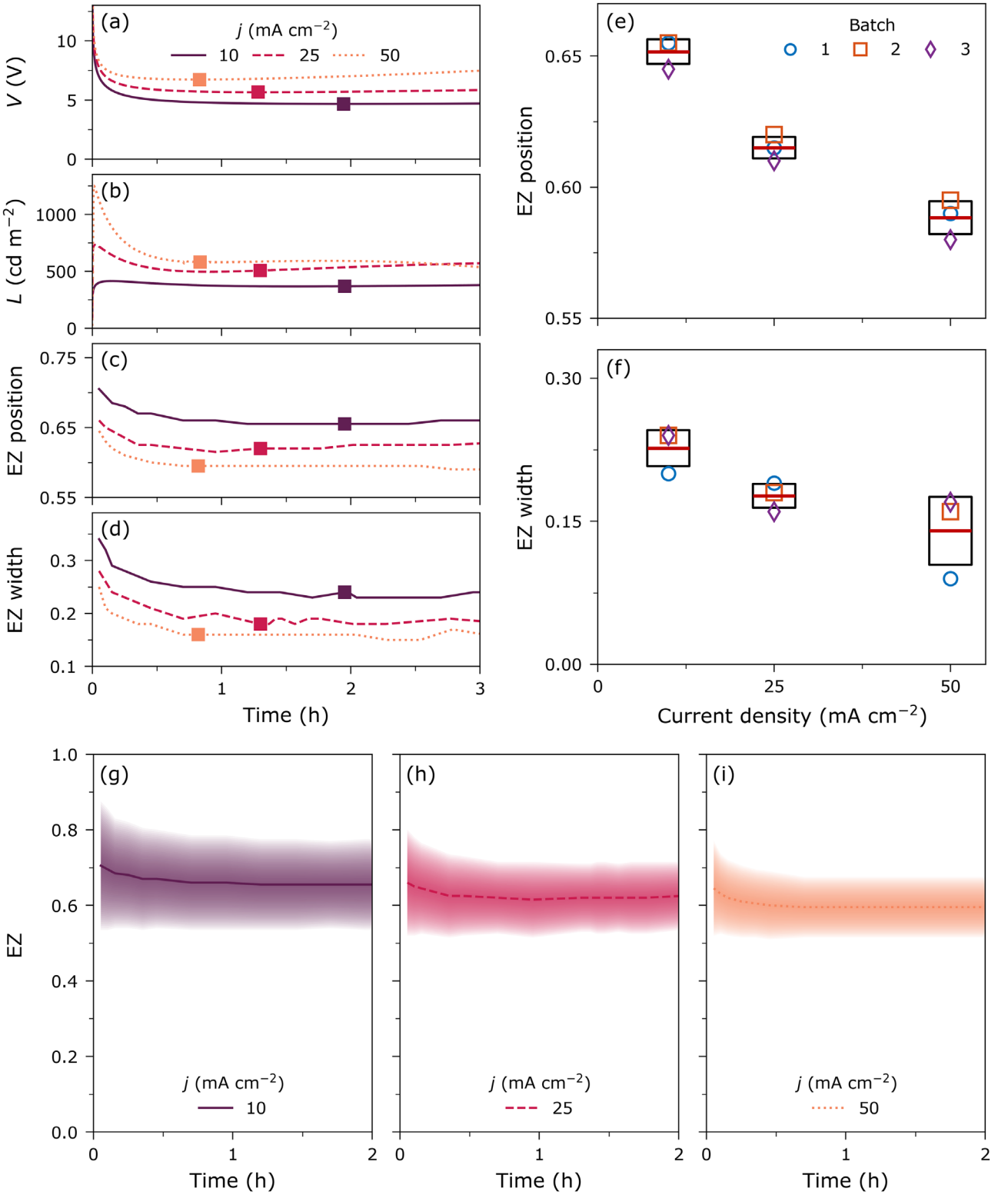

Figure 4. The temporal evolution of a) the voltage, b) the forward luminance, c) the best-estimated EZ position, and d) the best-estimated EZ width for typical LEC devices of batch 2 when driven by a constant current density, as identified in the inset of (a). The solid squares indicate the time of steady state, i.e., minimum voltage. e) The steady-state values for the best-estimated EZ position and f) the best-estimated EZ width for the three different LEC batches as a function of the current density. The red horizontal line markers show the mean value and the black rectangles show the population standard deviation, as calculated from the best-estimated EZ position and the best-estimated EZ width of the three batches. g–i) The temporal evolution of the best-estimated EZ position (line) and the best-estimated EZ width (shaded area) at three different current densities, as indicated in the insets.

To facilitate a discussion of the collected data, Figure 4g–i visualize the combined temporal evolution of the EZ center position and the EZ width at the three current densities. For the analysis, we first call attention to that it has been demonstrated that the initial EZ position will form closer to the negative cathode when the cation mobility is higher than the anion mobility; whereas a cathodically displaced steady-state EZ position originates in that the hole mobility is higher than the electron mobility.[23,35] Thus, the observation that the initial EZ position invariably forms closer to the cathode shows that the cations are more mobile than the anions, whereas the steady-state formation of the EZ position closer to the cathode is due to that the holes are more mobile than the electrons. Moreover, the observed shift of the steady-state EZ toward the positive anode with increasing current density (and voltage) implies that the positive dependency on the E-field is higher for the electron mobility than the hole mobility.

We further rationalize the observed decrease of the EZ width during the initial LEC operation by that the electrochemical doping processes are still ongoing in this time window, which will be manifested in a gradual increase of the overall doping concentration and a gradual thinning of the EZ (and the p-n junction).[52] The final observation, that the steady-state width of the EZ is decreasing with increasing current density, is at this stage less straightforward to explain, but we note with interest that earlier investigations, using impedance spectroscopy,[53,54] have reported on a similar thinning of the EZ with increasing current density.

We conclude with a short discussion of the implications of our specific findings. First, the observed temporal shift of the EZ position toward the center of the interelectrode gap results in the outcoupling efficiency for this particular device structure is decreasing with operational time, as displayed in Figure S4a (Supporting Information). This observation explains, in part, why the forward luminance of the LEC driven by the two higher current densities in Figure 4b is decreasing during the initial operation. Similarly, the shift of the steady-state EZ position toward the center of the gap with increasing current density also results in a significant relative lowering of the outcoupling efficiency by ≈30%, as displayed in Figure S4b (Supporting Information).

Finally, the observation of a decreasing EZ width with increasing current density is highly relevant in the context of the LEC emission efficiency and the efficiency roll-off. More specifically, a narrowing of the EZ will result in an increase of the emission losses to exciton-exciton quenching and exciton-polaron quenching,[28] and therefore result in an increased efficiency roll-off. Thus, the presented method for the determination of the dynamic EZ width and position in operating LEC devices can contribute to the appropriate and more exact identification of loss channels, and, as such, enable for a rational design of improved devices.

3. Conclusion

We present a method for the in-situ determination of the temporal evolution of the EZ width during LEC operation, which constitutes a fitting of simulated angular-resolved EL spectra to the corresponding measured EL spectra, using the EZ width as a free parameter. For improved accuracy, the measurements utilize an outcoupling structure and the selective detection of s-polarized EL, while the simulation considers the wavelength- and doping-dependent refractive index. We test the presented method on a common conjugated-polymer LEC with an active-material thickness of 300 nm and establish that the EZ width decreases during the initial operation. We further find that the EZ width is ≈20% of the active-material thickness during steady-state operation at a current density of 10 mA cm^{-2}, but that the steady-state EZ width appears to decrease with increasing current density. We note that such a decrease of the EZ width can be expected to be concomitant with increased exciton quenching. Thus, we anticipate that the presented method for determining the elusive EZ width in sandwich-cell LECs can contribute to a better understanding of the LEC operation and to the rational design of improved devices.

4. Experimental Section

The electroluminescent organic semiconductor was a phenyl-substituted poly (paraphenylene vinylene) conjugated copolymer termed "Super Yellow" (average repeat unit: 338 g mol^{-1}, M_n >400,000 g mol^{-1}, M_w >1 300 000 g mol^{-1}. trade name: PDY-132, Merck), the salt was KCF_3SO_3 (purity: 99.5%, SOLVIONIC), and the ion transporter was hydroxyl-capped trimethylolpropane ethoxylate (TMPE-OH, M_n = 450 g mol^{-1}, Sigma–Aldrich). The salt and the ion transporter were dried for 12 h in a vacuum oven at 190 and 50 °C, respectively, while Super Yellow was used as received. The active-material constituents were separately dissolved in cyclohexanone (purity ≥ 99.5%, Sigma–Aldrich) in the following concentrations: KCF_3SO_3 and TMPE-OH: 10 g l^{-1}; Super Yellow: 12 g l^{-1}. These master solutions were stirred on a magnetic hot plate at 70° for ≥ 12 h. The salt solution was additionally filtered through a 0.1 µm polytetrafluoroethylene syringe filter (Whatman Puradisc 25, Cytiva). The active-material ink was prepared by blending the master inks in a mass ratio of Super Yellow:TMPE-OH:KCF_3SO_3 = 1:0.1:0.03, followed by stirring on a hot plate at 70 °C for ≥ 6 h before further use.

The LEC devices were fabricated on transparent indium-tin-oxide (ITO) coated glass substrates (ITO thickness = 145 nm, R_s = 15 Ω $\square^{-1}$, glass thickness = 0.70 mm, substrate area = 30.0 × 30.0 mm^2, Kintec). The ITO substrates were cleaned by sequential ultrasonic treatment in detergent (Extran MA 01, Merck), deionized water, acetone, and isopropanol, followed by drying in an oven at 120 °C for ≥ 1 h. The active-material ink was spin-coated (ramp-up time = 1 s, spinning speed = 1500–1600 rpm, spinning time = 120 s) on the ITO, and the deposited active-material film was dried at 70 °C for 1 h. The dry thickness of the active material was 300 ± 10 nm, as measured with a stylus profilometer (DektakXT, Bruker). The reflective Al top electrode (thickness = 100 nm) was deposited by thermal evaporation under vacuum ($p < 8 \times 10^{-6}$ mbar) through a shadow mask. The overlap of the transparent ITO anode and the reflective Al cathode defined four independent 2.0 × 2.0 mm^2 LEC devices on each substrate. The LECs were protected from the ambient air by attaching a thin glass plate on top of the Al cathodes with a UV-curable epoxy (E132, Ossila), which was cured by exposure to UV light for 30 min (UV-Exposure Box 1, Gie-Tec GmbH). The ink preparation and the device fabrication were performed in N_2-filled gloveboxes ($[O_2]$ < 1 ppm, $[H_2O]$ < 1 ppm).

The angle-dependent EL spectrum and intensity were measured with a custom-built and automated spectrogoniometer setup, as controlled by a computer (Raspberry Pi 400) and a Python-based virtual instrument.[36] The LEC device under study was placed at the center of a goniometer stage, which rotation defined the emission angle. An emission angle of 0° corresponds to the forward direction, and the EL data were recorded for angles ranging from −86.4° to 86.4° in increments of 5.4°. A half-cylinder glass lens (radius = 20 mm, focal length = 40 mm), with its symmetry axis aligned with the rotation axis of the stage, was attached to the glass substrate of the device by an index-matching oil (n = 1.516, OIL-8CC, Olympus). The device was electrically driven and measured by source-measure unit (Keithley 2400), with the compliance voltage being 21 V. A fraction

of the emitted light was collected by a collimating lens (∅ = 7.2 mm, NA = 0.38, F110SMA-532, Thorlabs), with a collection angle of 0.004 sr and placed 100 mm away from the device surface. An optical fiber (∅ = 600 µm, NA = 0.39, M29L01, Thorlabs) delivered the collected light to a CCD-array spectrometer (FLAME-S-XR1-ES, Ocean Optics). A linear polarizer (LPVISE100-A, Thorlabs), which only allowed s-polarized light to pass through, was placed in front of the detector.

The optical modeling was performed with a commercial software (Setfos, versions 5.2/5.3 Fluxim AG, CH). The simulated LEC device structure, as displayed schematically in Figure 2a, comprised an Al top cathode (thickness = 100 nm), the active material (thickness = 300 nm), an ITO anode (thickness = 145 nm), and an infinitely thick glass substrate. The simulated doping and exciton generation profiles in the active material during steady-state operation are presented in Figure 2b, and the doping profiles are described in detail in the accompanying text. The exciton generation profile was simulated as a Gaussian function (see Equation 1), with the peak position at x_0 and the standard deviation being σ. The EZ position was equal to x_0, while the EZ width, w_0, was set equal to 6σ. Since the model does not permit emission to take place in absorbing (here doping) regions, the EZ was modelled as being non-absorbing (i.e., transparent). Since only the s-polarized light was detected in the angle-dependent experiment, information on the optical anisotropy of the emitter was irrelevant.[36] The restriction was finally imposed in the modeling that the EZ width could not exceed 50% of the active material thickness, since this resulted in a doping concentration at the electrode interfaces that was larger than the available density of the states of the organic semiconductor Super Yellow. The two free parameters in the fitting of the simulated EL data to the measured EL data are x_0 and $w_0 = 6\sigma$ (as normalized to the active-material thickness of 300 nm); and x_0 was changed from 0.005 and 0.995 in steps of 0.005, while w_0 was varied between 0.01 to 0.50 in steps of 0.01, which resulted in a set of 199×50 solutions for $I^{\mathrm{sim}}_{\theta,\lambda}(x_0, w_0)$ in Equation (2). By using the solution landscape at the expense of a finite resolution of the free parameters, the speed of the fitting procedure was improved, the risk of reaching a local minimum was suppressed and especially the goodness of the fit was visualized in a very clear way.

5. Statistical Analysis

Nine nominally identical LEC devices were fabricated and measured, and the observed variation in the spectral and optoelectronic performance were very minor, as detailed in Table S1 (Supporting Information).

Supporting Information

Supporting Information is available from the Wiley Online Library or from the author.

Acknowledgements

The authors acknowledge financial support from the Swedish Research Council (2019-02345 and 2021-04778), the Kempe Foundations, and the Wallenberg Initiative Materials Science for Sustainability (WISE) funded by the Knut and Alice Wallenberg Foundation (WISE-AP01-D02). L.E. acknowledges financial support from the European Union through an ERC Advanced Grant (ERC, InnovaLEC, 101096650). A.K. acknowledges funding from the European Union (HORIZON MSCA 2023 PF, acronym UNID, grant number 101150699).

Conflict of Interest

The authors declare no conflict of interest.

Data Availability Statement

The data that support the findings of this study are openly available in Figshare at 10.6084/m9.figshare.28869602, reference number 28869602.

Keywords

dynamic doping, emission efficiency, emission zone width, light-emitting electrochemical cell, method development

Received: April 9, 2025
Revised: May 11, 2025
Published online: May 27, 2025

[1] J. Katsumata, F. Osawa, G. Sato, A. Sato, K. Miwa, S. Ono, K. Marumoto, *Commun. Mater.* **2023**, *4*, 41.
[2] Y. Shao, G. C. Bazan, A. J. Heeger, *Adv. Mater.* **2007**, *19*, 365.
[3] J. Liu, J. Wang, Z. Zhang, F. Molina-Lopez, G.-J. N. Wang, B. C. Schroeder, X. Yan, Y. Zeng, O. Zhao, H. Tran, T. Lei, Y. Lu, Y.-X. Wang, J. B. H. Tok, R. Dauskardt, J. W. Chung, Y. Yun, Z. Bao, *Nat. Commun.* **2020**, *11*, 3362.
[4] Z. Zhang, K. Guo, Y. Li, X. Li, G. Guan, H. Li, Y. Luo, F. Zhao, Q. Zhang, B. Wei, Q. Pei, H. Peng, *Nat. Photonics* **2015**, *9*, 233.
[5] H. L. Filiatrault, G. C. Porteous, R. S. Carmichael, G. J. E. Davidson, T. B. Carmichael, *Adv. Mater.* **2012**, *24*, 2673,.
[6] A. Sandström, A. Asadpoordarvish, J. Enevold, L. Edman, *Adv. Mater.* **2014**, *26*, 4975.
[7] E. Nannen, J. Frohleiks, S. Gellner, *Adv. Funct. Mater.* **2020**, *30*, 1907349.
[8] M. Chen, J. Ye, J. Lu, S. Wu, G. Lin, Y. Ma, L. Liu, Y. Zhang, L. Niu, B. Zhang, *Org. Electron.* **2025**, *142*, 107252.
[9] S. Tang, Y. Tsuchiya, J. Wang, C. Adachi, L. Edman, *Nat. Commun.* **2025**, *16*, 653.
[10] K. Zhang, X. Pang, Y. Song, Y. Xiu, R. Yu, L. He, *Adv. Opt. Mater.* **2024**, *12*, 2400467.
[11] J. Wang, H. Hafeez, S. Tang, T. Matulaitis, L. Edman, I. D. W. Samuel, E. Zysman-Colman, *Aggregate* **2024**, *5*, 571.
[12] K. Zhang, Y. Song, Y. Xiu, Y. Li, L. He, *Chem. Eng. J.* **2024**, *500*, 157429.
[13] Z. Zhou, Q. Chang, R. Chen, P. Jin, B. Yin, C. Zhang, J. Yao, *Phys. Chem. Chem. Phys.* **2024**, *26*, 24498.
[14] R. Yu, Y. Song, K. Zhang, X. Pang, M. Tian, L. He, I. Ionic, *Adv. Funct. Mater.* **2022**, *32*, 2110623,.
[15] S. Tang, L. Edman, *Top. Curr. Chem.* **2016**, *374*, 40.
[16] J. Zimmermann, S. Schlisske, M. Held, J.-N. Tisserant, L. Porcarelli, A. Sanchez-Sanchez, D. Mecerreyes, G. Hernandez-Sosa, *Adv. Mater. Technol.* **2019**, *4*, 1800641.
[17] E. Auroux, G. Huseynova, J. Ràfols-Ribé, V. Miranda La Hera, L. Edman, *RSC Adv.* **2023**, *13*, 16943.
[18] Q. Pei, G. Yu, C. Zhang, Y. Yang, A. J. Heeger, *Science* **1995**, *269*, 1086.
[19] T. Sakanoue, F. Yonekawa, K. Albrecht, K. Yamamoto, T. Takenobu, *Chem. Mater.* **2017**, *29*, 6122.
[20] R. Bai, P. Huo, N. Zheng, Y. Li, W. Yan, P. Fang, X. Zhou, Z. Bian, Z. Liu, *Adv. Mater.* **2025**, 2419849.
[21] R. D. Costa, D. Tordera, E. Ortí, H. J. Bolink, J. Schönle, S. Graber, C. E. Housecroft, E. C. Constable, J. A. Zampese, *J. Mater. Chem.* **2011**, *21*, 16108.
[22] Q. Pei, Y. Yang, G. Yu, C. Zhang, A. J. Heeger, *J. Am. Chem. Soc.* **1996**, *118*, 3922.
[23] J. Ràfols-Ribé, X. Zhang, C. Larsen, P. Lundberg, E. M. Lindh, C. T. Mai, J. Mindemark, E. Gracia-Espino, L. Edman, *Adv. Mater.* **2022**, *34*, 2107849.

[24] S. Jenatsch, L. Wang, N. Leclaire, E. Hack, R. Steim, S. B. Anantharaman, J. Heier, B. Ruhstaller, L. Penninck, F. Nüesch, R. Hany, *Org. Electron.* **2017**, *48*, 77,.
[25] S. Jenatsch, M. Regnat, R. Hany, M. Diethelm, F. Nüesch, B. Ruhstaller, *ACS Photonics* **2018**, *5*, 1591.
[26] Y. Li, B. Van der Zee, X. Tan, X. Zhou, G.-J. A. H. Wetzelaer, P. W. M. Blom, *Adv. Mater.* **2023**, *35*, 2304728.
[27] S. Tang, A. Sandstrom, P. Lundberg, T. Lanz, C. Larsen, S. van Reenen, M. Kemerink, L. Edman, *Nat. Commun.* **2017**, *8*, 1190.
[28] X. Zhang, J. Ràfols-Ribé, J. Mindemark, S. Tang, M. Lindh, E. Gracia-Espino, C. Larsen, L. Edman, *Adv. Mater.* **2024**, *36*, 2310156.
[29] A. Kirch, S.-R. Park, J. Ràfols-Ribé, J. A. Kassel, X. Zhang, S. Tang, C. Larsen, L. Edman, *ACS Appl. Mater. Interfaces* **2025**, *17*, 5184.
[30] B. Perucco, N. A. Reinke, D. Rezzonico, M. Moos, B. Ruhstaller, *Opt. Express* **2010**, *18*, A246.
[31] M. Furno, R. Meerheim, S. Hofmann, B. Lüssem, K. Leo, *Phys. Rev. B* **2012**, *85*, 115205.
[32] T.-W. Wang, H.-C. Su, *Org. Electron.* **2013**, *14*, 2269.
[33] S. van Reenen, R. A. J. Janssen, M. Kemerink, *Adv. Funct. Mater.* **2012**, *22*, 4547.
[34] S. Jenatsch, L. Wang, M. Bulloni, A. C. Véron, B. Ruhstaller, S. Altazin, F. Nüesch, R. Hany, *ACS Appl. Mater. Interfaces* **2016**, *8*, 6554.
[35] M. Diethelm, A. Schiller, M. Kawecki, A. Devižis, B. Blülle, S. Jenatsch, E. Knapp, Q. Grossmann, B. Ruhstaller, F. Nüesch, R. Hany, *Adv. Funct. Mater.* **2020**, *30*, 1906803,.
[36] J. Ràfols-Ribé, C. Hänisch, C. Larsen, S. Reineke, L. Edman, *Adv. Mater. Technol.* **2023**, *8*, 2202120.
[37] W. Brütting, J. Frischeisen, T. D. Schmidt, B. J. Scholz, C. Mayr, *Physica Status Solidi A* **2013**, *210*, 44.
[38] Y. Yamamoto, R. E. Slusher, *Phys. Today* **1993**, *46*, 66.
[39] D. G. Deppe, C. Lei, C. C. Lin, D. L. Huffaker, *J. Mod. Opt.* **1994**, *41*, 325.
[40] A. Dodabalapur, L. J. Rothberg, R. H. Jordan, T. M. Miller, R. E. Slusher, J. M. Phillips, *J. Appl. Phys.* **1996**, *80*, 6954.
[41] X. Liu, D. Poitras, Y. Tao, C. Py, *J. Vac. Sci. Technol. A* **2004**, *22*, 764.
[42] A. Chin, T. Y. Chang, *J. Lightwave Technol.* **1991**, *9*, 321.
[43] D. G. Lidzey, D. D. C. Bradley, S. J. Martin, M. A. Pate, *IEEE J. Sel. Top. Quantum Electron.* **1998**, *4*, 113.
[44] G. J. Lee, B. Y. Jung, C. K. Hwangbo, J. S. Yoon, *Jpn. J. Appl. Phys.* **2002**, *41*, 5241.
[45] C. Hänisch, S. Lenk, S. Reineke, *Phys. Rev. Appl.* **2020**, *14*, 064036.
[46] A. Dodabalapur, L. J. Rothberg, T. M. Miller, E. W. Kwock, *Appl. Phys. Lett.* **1994**, *64*, 2486.
[47] T. Lanz, E. M. Lindh, L. Edman, *J. Mater. Chem. C* **2017**, *5*, 4706.
[48] E. M. Lindh, P. Lundberg, T. Lanz, L. Edman, *Sci. Rep.* **2019**, *9*, 10433.
[49] L. Lin, S. Ke, W. Yang, Y. Zhang, Q. Cui, Z. Lou, Y. Hou, F. Teng, Y. Hu, *Org. Electron.* **2024**, *127*, 107007,.
[50] D. Wang, E. Desroche, J. Gao, *Adv. Mater. Interfaces* **2020**, *7*, 1901216.
[51] A. Sandström, P. Matyba, L. Edman, *Appl. Phys. Lett.* **2010**, *96*, 053303.
[52] N. D. Robinson, J. Fang, P. Matyba, L. Edman, *Phys. Rev. B* **2008**, *78*, 245202.
[53] Y. A. Davis, P. P. Crooker, N. M. Haegel, Y. Yoshioka, J. D. MacKenzie, *Appl. Phys. Lett.* **2011**, *99*, 233306.
[54] S. B. Meier, D. Hartmann, A. Winnacker, W. Sarfert, *J. Appl. Phys.* **2014**, *116*, 104504.